Phase-contrast tomography with low-intensity beams

J. Řeháček,[1] Z. Hradil,[1] M. Zawisky,[2] U. Bonse,[3] and F. Dubus[4]
[1]*Department of Optics, Palacký University, 17. listopadu 50, 772 00 Olomouc, Czech Republic*
[2]*Atominstitut der Österreichischen Universitäten, Stadionallee 2, A-1020 Wien, Austria*
[3]*Physics Department, University of Dortmund, Otto Hahn Straße 4, D-44221 Dortmund, Germany*
[4]*Atominstitut der Österreichischen Universitäten, Stadionallee 2, A-1020 Wien, Austria*
(Received 14 June 2004; published 16 February 2005)

In newly developed neutron phase tomography, wave properties of neutrons are exploited for the nondestructive testing of the internal structure of matter. We show how limitations due to small available intensities of present neutron sources can be overcome by using an advanced maximum-likelihood reconstruction algorithm. Unlike the standard filtered back-projection, the developed procedure gives reasonable results also when used on very noisy data or data consisting of only a few measured projections. This is demonstrated by means of simulations and also experimentally. The proposed method leads to considerably shorter measuring times and/or increased precision.

DOI: 10.1103/PhysRevA.71.023608 PACS number(s): 03.75.Dg, 81.70.Fy, 81.70.Tx

I. INTRODUCTION

In neutron optics one is often confronted with low count numbers because the phase space densities of present neutron beams is many orders of magnitude below that of laser and x-ray synchrotron beams. This intensity problem has dramatically arisen in the recently developed neutron phase contrast tomography (*n*PCT) [1]. PCT was originally invented in x-ray tomography with much higher intensities available [2–4]. In order to utilize *n*PCT it is necessary to develop an advanced maximum-likelihood (ML) reconstruction technique, which can be applied to very low count numbers. For instance, the typical count number in our present *n*PCT setup is about 100 $n/2h$ in a 50×50 μm^2 pixel. In principle focusing techniques, e.g., asymmetric Bragg reflections, can enhance the density of the quasimonochromatic and well-collimated neutron beams, but such hypothetic gains will rather be used to reduce the measurement time than to raise the count numbers. Therefore the low numbers of detected neutrons have to be accepted as the limiting factor of *n*PCT, and our strategy is to master the tomographic reconstruction even in that extreme case.

Our motivation for developing *n*PCT is its extreme sensitivity, which is at least three orders of magnitude higher than that of conventional transmission tomography. The *n*PCT method proves its strength in extreme applications where other methods fail: (i) 3D investigation of non- or weak-absorbing substances, (ii) analysis of isotope distributions with high sensitivity, (iii) investigation of magnetic domains in bulk materials, and (iv) energy and momentum exchange free analysis of magnetic (axial) and scalar potentials. In short, neutron phase tomography seems to be extremely useful for the investigation of internal structure in material science.

Our first results have been obtained using the standard filtered-backprojection (FB) method [5]. The tomographic projection of a scalar phase field can be described similar to a scalar density field. But there are important differences between phase and transmission tomography. Phases are not directly measurable, and they are restricted to the $[0,2\pi]$ interval.

In general, a set of reference phases controlled by the experimenter is needed for the estimation of phases. The use of an auxiliary phase shifter δ_j is routinely applied in neutron interferometry and the resulting phase shifter interferograms are simply called scans [6]. In principle only two reference phases are needed for the unique phase determination in the $[0,2\pi]$ interval. But our choice of three reference phases ($\delta_j=0°,120°,240°$) has several advantages. It will be shown later that for three reference measurements an analytical evaluation of the unknown parameters (phase, visibility, mean number) is possible. Generalization to an arbitrary large set of auxiliary phases was given in [7]. However, since the total measurement time is proportional to the number of scans taken and the currently available coherent neutron intensities are low, small sets of reference phase measurements are preferred.

The second difference is directly related to the FB method, where the accumulated phases are the starting point for tomographic reconstruction. Due to the high phase sensitivity it is very likely that the projected phases exceed 2π, which requires an additional phase correction before applying the conventional FB routine.

Other FB shortcomings should be addressed shortly. The image quality depends strongly on the filter parameters and has not the objectivity of the presented ML method. Additionally, noise gets amplified in the standard FB filters [8]. It was demonstrated in [9] that the standard FB routine fails for strongly fluctuating data. The FB algorithm requires equidistant projection angles covering the full 180° interval. If one projection is missing or contains bad data, then the whole reconstruction fails. Poor results are obtained if only a few projections are available. These FB constraints hinder the full exploitation of neutron tomography, therefore a ML reconstruction algorithm has been developed, which overcomes the FB shortcomings mentioned.

This paper is organized as follows: In Sec. II we discuss in detail the estimation of the total phase accumulated in a sample. In Sec. III our maximum-likelihood algorithm for the phase-contrast tomography is derived. Optimal treatment of reference phase measurements leading to a refined reconstruction routine is discussed in Sec. IV. In Sec. V we apply

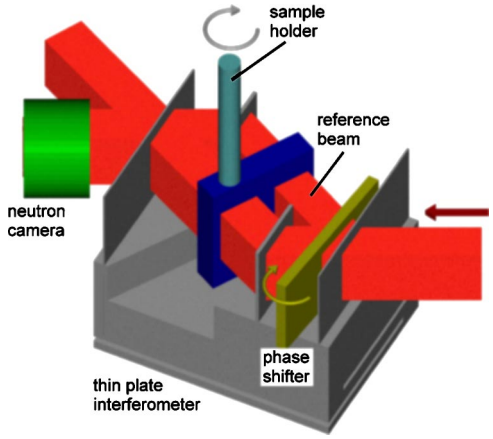

FIG. 1. Scheme of *n*PCT experiment.

our procedure to data simulating extreme experimental conditions as well as to experimental data. We close with the summary of results in Sec. VI.

II. *n*PCT AND PHASE ESTIMATION

For independent measurements, as it is the case for Poissonian statistics, all the accumulated information can be expressed as an *a posteriori* likelihood function. It is essential that the likelihood includes all measured data, and, together with the physical model for the detection probabilities, all experimental information. Thus the likelihood is the optimum starting point for a complete tomographic analysis.

The experimental setup of *n*PCT is schematically shown in Fig. 1. The sample is inserted into one arm of a perfect crystal interferometer while an object of known characteristics placed in the other arm compensates the large overall phase shift introduced by the thick sample. The output beam is then registered by a CCD camera with the spatial resolution of 50 μm. Like in absorption tomography, the sample is rotated around the vertical axis and up to several tens of scans are registered. Angle φ together with the position h of a CCD pixel specify the path of the particles registered by that pixel through the sample; see Fig. 2. For the sake of brevity, h and φ will be represented by a single collective index j. To get an unambiguous value of the reconstructed phase, each scan is repeated several times with different settings of the auxiliary phase shifter.

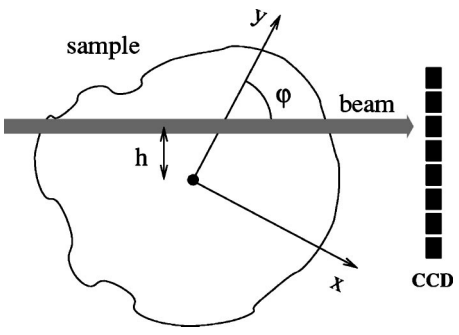

FIG. 2. Geometry of a tomographic imaging.

*n*PCT involves two nontrivial inverse problems: phase estimation and tomographic imaging. Let us first discuss the former one and justify our particular choice of auxiliary phases. Consider an interferometric measurement with intensity N and amplitude V. The measured interference pattern,

$$\overline{n_\alpha}(\overline{\theta}) = N + V\cos(\overline{\theta} + \delta_\alpha), \tag{1}$$

depends on the true value $\overline{\theta}$ of the sought after phase. To estimate it, the interference pattern will be scanned with L different settings of the auxiliary phase shifter uniformly distributed over the 2π phase window,

$$\delta_\alpha = \alpha\frac{2\pi}{L}, \quad \alpha = 0,1,\ldots,L-1. \tag{2}$$

If thermal phase drifts are negligible, then the only fluctuating quantity in a tomographic measurement is the count number of particles. Its fluctuations are described by the Poissonian statistics, which was confirmed in several experiments [10,11]. Since the detections with different settings δ_α are statistically independent events, the joint probability of registering data **n** is simply a product of Poissonian likelihood functions,

$$\mathcal{L}(\theta) = \prod_\alpha \frac{\overline{n}_\alpha^{n_\alpha}(\theta)}{n_\alpha!} e^{\overline{n}_\alpha(\theta)}. \tag{3}$$

This is also the likelihood of a given value θ of the unknown phase shift.

In accordance with the maximum likelihood principle, we will take the maximum likely phase as the inferred value of θ. This value is found by maximizing function (3) or its logarithm. In the case of uniformly distributed auxiliary phase shifts, when the identity $\Sigma_\alpha \cos(\theta+\delta_\alpha)=0$ holds, the log-likelihood simplifies to

$$\log\mathcal{L} = \sum_\alpha n_\alpha \log[N + V\cos(\theta+\delta_\alpha)] - NL. \tag{4}$$

At this point it is convenient to introduce new variables $x = V\cos\theta$ and $y = V\sin\theta$. We are looking for the point where the likelihood has zero slope: $\partial\mathcal{L}/\partial x = \partial\mathcal{L}/\partial y = \partial\mathcal{L}/\partial N = 0$. From Eq. (4) we get the following extremal equations:

$$\sum_\alpha \frac{n_\alpha \cos\delta_\alpha}{N + x\cos\delta_\alpha - y\sin\delta_\alpha} = 0,$$

$$\sum_\alpha \frac{n_\alpha \sin\delta_\alpha}{N + x\cos\delta_\alpha - y\sin\delta_\alpha} = 0, \tag{5}$$

$$\sum_\alpha \frac{n_\alpha}{N + x\cos\delta_\alpha - y\sin\delta_\alpha} = L.$$

In general, these equations have to be solved numerically, for instance by some iterative procedure. However, there is one special case where the solution of Eq. (5) can be obtained in a closed form. This solution is related to another estimation problem—phase estimation in the presence of Gaussian signal. The likelihood (3) is consistent with the fact that the detected signal consists of discrete particles. Now consider a

thought experiment with Gaussian signal described by the likelihood

$$\mathcal{L} = \prod_{\alpha} \exp(-(\overline{n_\alpha} - n_\alpha)^2/\sigma^2). \tag{6}$$

In this case, all measured quantities are affected by the same amount of noise σ, no matter what the true values of the estimated parameters are. Such behavior would be typical for continuous signal (waves). As can be easily checked, Gaussian likelihood (6) is maximized by the quadratic estimator (least square fit):

$$x = 2\sum_{\alpha} n_\alpha \cos(-\delta_\alpha)/L,$$

$$y = 2\sum_{\alpha} n_\alpha \sin(-\delta_\alpha)/L, \tag{7}$$

$$N = \sum_{\alpha} n_\alpha/L,$$

which, going back to the original variables, can be written in the following compact form:

$$V = 2|R|/L, \quad e^{i\theta} = R/|R|, \tag{8}$$

where

$$R = \sum_{\alpha} n_\alpha e^{-i\delta_\alpha} \tag{9}$$

is the first coefficient of the discrete Fourier transformation (DFT) of the registered counts n_α [12]. Now since the Gaussian assumption about the detected signal is only an approximation to the true statistics [13,14], the estimator (8) will generally not be the optimal one. However, one can easily verify, that if three auxiliary phase shifts are used ($L=3$), the solution (7) will also satisfy the Poissonian extremal equations (5). This means that it is particularly useful to use three auxiliary phase shifts for in that case the optimal phase estimation is easily done by means of the simple analytical formula (8).

III. MAXIMUM-LIKELIHOOD *n*PCT ALGORITHM

In *n*PCT, phase sensitive data $n_{j\alpha}$ are registered. Indexes j and α label scans (i.e., pixels of the CCD camera and rotations of the sample) and auxiliary phases, respectively. Since each scan contributes likelihood (6) and different scans are independent observations, the total likelihood reads

$$\log \mathcal{L} = \sum_{j} \sum_{\alpha} (n_{j\alpha} - \overline{n_{j\alpha}})^2. \tag{10}$$

Again, the mean numbers of particles detected in jth scan form an interference pattern,

$$n_{j\alpha} = N_j + V_j \cos(\theta_j + \delta_\alpha + \theta_j^r), \tag{11}$$

where the total phase accumulated along the jth projection is discretized as follows:

$$\theta_j = \sum_i c_{ji}\mu_i. \tag{12}$$

Here the coefficient c_{ji} quantifies the overlap between the jth projection and the ith elementary cell of the reconstruction mesh. Reference phases θ_j^r appearing in Eq. (11) describe the phase properties of the interferometer alone. They can be estimated from the same set of projections measured with the sample removed.

Likelihood (10) is to be maximized over the distribution μ_i of the scattering density in the sample. In neutron phase imaging, μ is given by the sum of scattering length densities (Nb) of all P isotopes comprising the sample:

$$\mu = -\lambda \sum_{l=1}^{P} N_l b_l = -\lambda \sum_{l=1}^{P} \frac{N_A \rho_l b_l}{A_l}. \tag{13}$$

Here N_l represents the number of isotopes l per unit volume, ρ_l the isotope density, N_A the Avogadro constant $[6.02214199(47)\times 10^{23}\ \mathrm{mol}^{-1}]$, and A_l the atomic weight. λ represents the mean wavelength of the illuminating quasimonochromatic beam, and b_l the coherent scattering length, which is a constant interaction parameter accurately known for most isotopes [15]. Most of them have a positive coherent scattering length but some are known with negative b_ls. The coherent scattering length is defined positive for repulsive optical potentials $\overline{V} > 0$ with the index of refraction less than unity: $n = \sqrt{1 - \overline{V}/E} = 1 - \lambda^2 N b_l / 2\pi$. The existence of positive and negative phase shifts is a specialty of neutron optics. It can be utilized for fading out unwanted phase contributions.

Using Eqs. (10) and (11) in the extremal conditions

$$\frac{\partial \mathcal{L}}{\partial \mu_i} = 0, \ \forall\ \mu_i, \tag{14}$$

we get

$$\mu_i = \mu_i \frac{\sum_j V_j c_{ji} \sin\theta_j \,\mathrm{Im}\{R_j\}}{\sum_j V_j c_{ji} \cos\theta_j \,\mathrm{Re}\{R_j\}}. \tag{15}$$

This set of nonlinear equations for the unknown distribution of μ_j is the main theoretical result of this paper. Notice that the system Eq. (15) has been put in a form suitable for iterations. Starting from some initial distribution of scattering density μ_i, the maximum-likely distribution is obtained by repeated iterations. This will be illustrated in Sec. V. A uniform distribution of μ_i makes usually a good starting point, but other choices may be used as well, especially if some prior knowledge about the geometry or composition of the sample is available.

IV. REFERENCE PHASES

No interferometers are perfect. Already an empty interferometer shows nonuniform distribution of phase difference between its two arms. To remove this background phase, the phase measurement is done in two steps: With the sample

and without it. The most simple way how to proceed is to determine the reference phase separately and then subtract it from the total phase as it is indicated in Eq. (11). This procedure is simple but not optimal. It is not difficult to see why. The inspection of Eq. (15) shows that the reconstructed indexes of refraction μ_i depend on the visibilities $v_j = V_j/N_j$ of the registered interference fringes. This is natural since phase tomography is a synthesis of many phase measurements, of which those having higher visibilities are less affected by noise and thus also lead to a more credible phase estimation. Similar argument applies to the reference phase measurement. Experimental conditions during the reference phase measurement are usually more favorable than that during the sample measurement. Consequently, the phase introduced by an empty interferometer is known to a greater accuracy than phase introduced by interferometer *and* sample. This additional knowledge can be incorporated into the reconstruction routine. Let us first rewrite the Gaussian posterior phase distribution Eq. (6) to a more compact form. Only its phase dependent part is now of importance,

$$\begin{aligned}\mathcal{L}(\theta) &\propto \exp\left[\frac{2V}{\sigma^2}\sum_\alpha n_\alpha \cos(\theta+\delta_\alpha)\right] \\ &= \exp\left[\frac{2V}{\sigma^2}\left(\cos\theta\sum_\alpha n_\alpha\cos\delta_\alpha - \sin\theta\sum_\alpha n_\alpha \sin\delta_\alpha\right)\right] \\ &= \exp\left[\frac{2V}{\sigma^2}(\mathrm{Re}\{R\}\cos\theta + \mathrm{Im}\{R\}\sin\theta)\right] \\ &= \exp\left[\frac{2V|R|}{\sigma^2}\cos(\theta-\theta_{\mathrm{DFT}})\right] = \exp[V^2\cos(\theta-\theta_{\mathrm{DFT}})].\end{aligned} \tag{16}$$

In the last step we have used Eq. (8), and set the unimportant scaling factor $L/\sigma^2 = 1$. Denoting now $\theta = \theta_s + \theta_r$ the total phase measured with the sample, which is the sum of the reference phase θ_r and phase θ_s introduced by the sample alone, the posterior distributions of θ and θ_r read

$$P(\theta) \propto e^{V^2\cos(\theta-\theta_{\mathrm{DFT}})}, \tag{17}$$

$$P(\theta_r) \propto e^{V_r^2\cos(\theta_r-\theta_{r,\mathrm{DFT}})}. \tag{18}$$

These are the standard von Mieses normal distributions defined on a unit circle. As has been mentioned above, given mean intensities, the widths of the phase distributions are determined by the corresponding visibilities. In *n*PCT we are interested only in phase θ_s introduced by the sample alone. The posterior distribution of θ_s can be readily obtained from Eq. (17) as a phase difference distribution,

$$P(\theta_s) = \int\int P(\theta)P(\theta_r)\delta(\theta-\theta_r-\theta_s)d\theta_r d\theta. \tag{19}$$

The double integrations can be easily carried out and the result expressed in terms of the Bessel function I:

$$P(\theta_s) \propto I_0(\sqrt{V^4 + V_r^4 + 2V^2V_r^2\cos(\theta_s - \theta_{-,\mathrm{DFT}})}), \tag{20}$$

where $\theta_{-,\mathrm{DFT}} = \theta_{\mathrm{DFT}} - \theta_{r,\mathrm{DFT}}$. This means that the phase measurements with the sample and without it, when taken together, amount to a single phase measurement with a modified visibility. This new effective visibility governing the phase resolution of the experiment can be determined from Eq. (20). In the limit of large count numbers, when the asymptotic expression

$$\lim_{x\to\infty} I_0(x) = \frac{e^x}{\sqrt{2\pi x}} \tag{21}$$

for the Bessel function holds, and assuming that $V_r \gg V$ as it is often found in experiments, Eq. (20) reduces to the von Mieses normal form, and the effective visibility v' becomes

$$v' \approx \frac{vv_r}{\sqrt[4]{v^4 + v_r^4}}. \tag{22}$$

Notice that $v' \to v$ as $v \to 0$. The error of the reference phase measurement can be ignored if the measurement with the sample is very noisy.

The total phase θ_{sj} accumulated along the jth projection can be written, as before, as a sum of the individual contributions from different cells, $\theta_{sj} = \Sigma c_{ij}\mu_i$. The posterior distribution Eq. (20) is then to be maximized over those μ_i. This leads to a refined *n*PCT reconstruction algorithm

$$\mu_i = \mu_i - (C_i - S_i)\mu_i, \tag{23}$$

where

$$C_i = \sum_j V_j^2 V_{rj}^2 I_1(x_j)\cos(\theta^j_{-,\mathrm{DFT}})/x_j, \tag{24}$$

$$S_i = \sum_j V_j^2 V_{rj}^2 I_1(x_j)\sin(\theta^j_{-,\mathrm{DFT}})/x_j, \tag{25}$$

and

$$x_j = \sqrt{V_j^4 + V_{rj}^4 + 2V_j^2V_{rj}^2\cos(\theta_j - \theta^j_{-,\mathrm{DFT}})}. \tag{26}$$

V. RESULTS

The presented theory has been extensively tested by means of computer simulations and also experimentally. The simpler of the two presented reconstruction algorithms Eq. (15) has been used for data processing since the error of the reference phase measurement could be ignored in our experiments. Of course, any real *n*PCT experiment is more complicated than the simple ideal model discussed above, due to various sources of noise and presence of systematic errors. The power of the reconstruction method is fully revealed only in simulations.

Figure 3 shows a simulation of an ideal *n*PCT experiment under various experimental conditions. The artificial object shown in panel (a) was scanned from 31 different angles with the horizontal resolution of 81 pixels. Case (d) is the most interesting one. Here the simulated incident beam had such a low intensity that its Poissonian fluctuations were

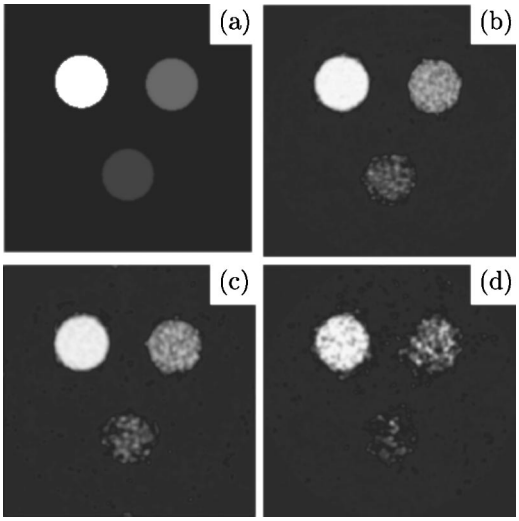

FIG. 3. Simulated phase tomography with a weak neutron signal. The maximal accumulated phases θ_j in the three cylinders making up the object (a) are 150°, 50°, and 30° for white, light gray, and dark gray cylinder, respectively. The simulated data consists of 31 projections, 81 pixels each, with the mean count numbers per pixel and visibilities as follows: (b) $N=450$, $v=33\%$; (c) $N=150$, $v=33\%$; (d) $N=30$, $v=33\%$.

comparable to the modulation caused by the maximal phase shifts introduced by the light gray and dark gray cylinders. Despite the useful phase information is thus nearly lost in the background noise, all three cylinders nicely show in the reconstruction.

Another example is shown in Fig. 4. Simulated experimental conditions are similar to those of Fig. 3 except for the maximal phase shifts that are now well in excess of 4π radians. This prior knowledge could be easily incorporated into the reconstruction, and as a result, the internal structure of the object was nicely resolved.

An isotope gauge with a similar geometry has been investigated at the *n*PCT setup in the Institute Laue-Langevin in Grenoble [16] in order to test the method and verify its sensitivity and spatial resolution under realistic conditions. The test object was an aluminum rod of 7 mm diameter with three cylinders drilled in, filled with different isotope mixtures; see Fig. 5(a). The central cylinder was filled with the mixture of 78% of elemental sulphur and 22% of aluminum oxide. The two smaller side holes were filled with two different water mixtures: 96% H_2O+4% D_2O and 95.6% H_2O+4.4% D_2O. Notice that both the sulfur isotopes and the aluminum are nearly transparent to thermal neutrons and therefore invisible in conventional transmission tomography shown in Fig. 5(b).

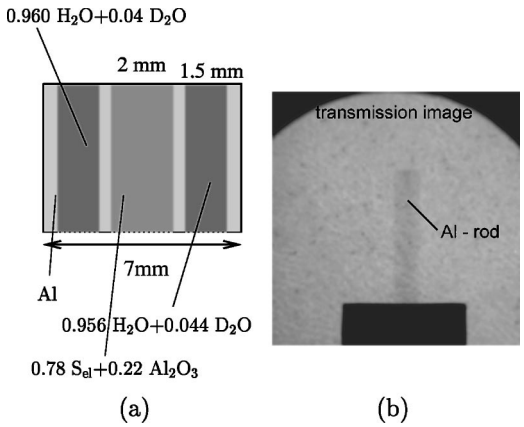

FIG. 5. Side view of the measured sample: (a) schematic picture; (b) conventional transmission image.

In contrast to this, a sensitivity in detecting nuclear density differences at a 1% level has been confirmed in the phase analysis, with a spatial resolution of 50 μm in the phase projections.

Tomographic reconstructions from the measured phase sensitive data are summarized in Fig. 6. Panel (a) is a picture of the top of the sample showing its true geometry. For the reconstruction, 30 different projections were measured with the transversal resolution of about 150 pixels per the width of the aluminum rod. Intensity in the region of interest was extremely low, typically below 30 counts per pixel. Small number of projections together with low intensity and small visibility (caused by scattering effects) make the data inversion a challenge for any reconstruction technique.

Panel (b) in Fig. 6 shows a typical maximum-likelihood reconstruction of a single 50 μm thick sample slice. Though the noise in the image is rather large, one can easily distin-

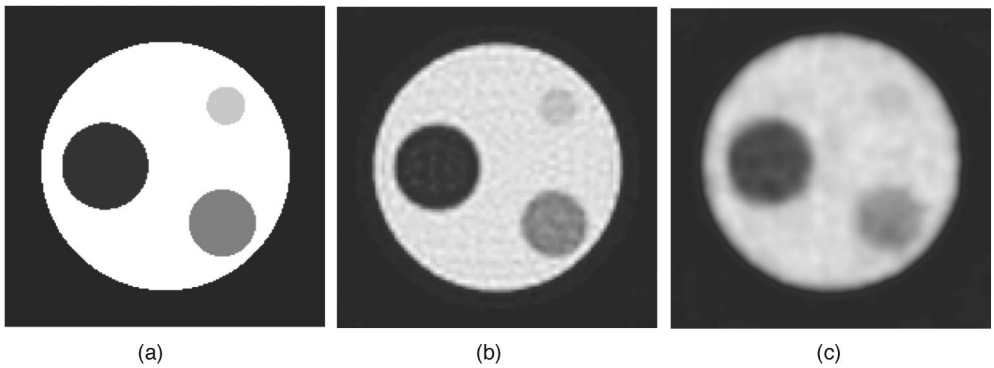

FIG. 4. Simulated phase tomography with a weak neutron signal, $N=150$ and $v=33\%$. The maximal accumulated phase θ_j in the object is 4.2π rad. (a) The artificial object; the ratio of the indexes of refraction in the white, light gray, dark gray, and black regions is 1:0.8:0.5:0.2. (b) ML reconstruction from 31 angles and 81 pixels. (c) ML reconstruction from 21 angles and 41 pixels.

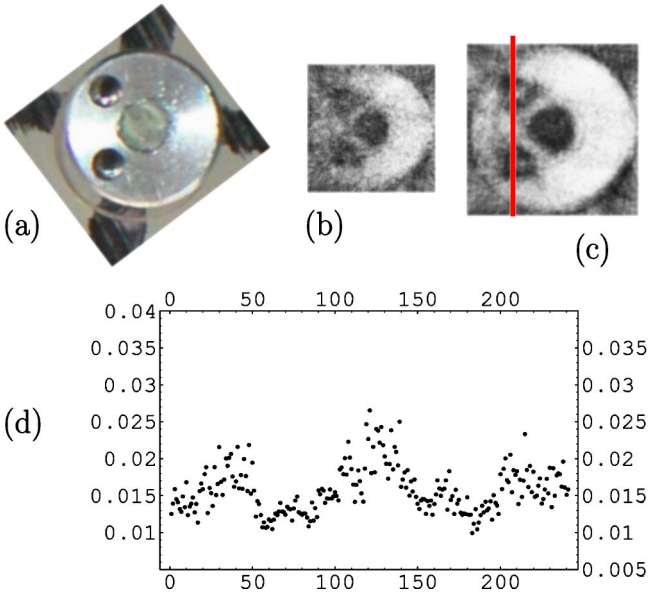

FIG. 6. Experimental maximum-likelihood *n*PCT: (a) top view of the sample; (b) typical reconstruction of a single 50 μm thick slice; (c) the same as (b) but data from 10 adjacent slices were collected prior to reconstruction; (d) line profile of the reconstructed scattering density (in arbitrary units) along the direction indicated in (c)

guish the geometry of the object. Still better results were obtained by using data averaged over 10 adjacent slices for the reconstruction (with the corresponding vertical resolution of 0.5 mm). In this way, the signal-to-noise ratio was somewhat increased. The resulting reconstruction is shown in Fig. 6(c). Last panel Fig. 6(d) shows the line profile of the reconstructed scattering density along the direction indicated by the vertical line in Fig. 6(c). The average scattering density in the two water isotope mixtures differs only by 10%, well in accordance with the expected values from the sample preparation. This relates to a sensitivity of 4×10^{-3} in the detection of D_2O differences in the mass fraction.

Finally, let us stress that we applied our algorithm to raw measured data without any prior filtering. The appearance of some artifacts in the reconstructed images (white specks inside the water cylinders) is probably caused by not considering scattering effects. However, given the extreme experimental conditions and the small number of measured projections, the reconstructions can be considered successful. Further enhancements can be expected after developing more accurate physical model of the experiment and applying appropriate filters prior to reconstruction.

VI. CONCLUSION

We have developed a new algorithm for phase-contrast tomography. Important features of this method are the following: (1) The two subproblems of the *n*PCT problem—phase estimation and tomographic imaging—are solved simultaneously, not one after the other. (2) All sources of noise can be incorporated into the model in a natural way. The method provides optimal treatment of noisy data. We have demonstrated its robustness in the extreme cases of small numbers of measured projections, low available intensities, and large total phase shifts induced by measured objects. In all cases our method yielded satisfactory results. As future *n*PCT applications we consider the analysis of weak absorbing substances and isotope distributions, and the sensitive detection of residues and corrosion in metals. The methods can be used in x-ray PCT as well, e.g., in medical imaging, where the absorbed radiation doses can significantly be reduced with the optimized maximum-likelihood routine.

ACKNOWLEDGMENTS

We are grateful to R. Loidl for helping us with the experiment. J.Ř. wishes to acknowledge the kind hospitality during his visits to ATI. We acknowledge the financial support from EURATOM-ÖAW, UT4-Underlying Technology project, from Grant No. LN00A015 of the Czech Ministry of Education, and from the East-West program of the Austrian Government.

[1] F. Dubus, U. Bonse, M. Zawisky, M. Baron, and R. Loidl, *First Phase-Contrast Tomography with thermal neutrons*, 7th World Conference on Neutron Radiography [IEEE Trans. Nucl. Sci. (Special Issue) (to be published)].
[2] A. Momose, Nucl. Instrum. Methods Phys. Res. A **352**, 622 (1995).
[3] A. Momose, T. Takeda, Y. Itai, and K. Hirano Nat. Med. **2**, 473 (1996).
[4] F. Beckmann, U. Bonse, F. Busch, and O. Gnnewig, J. Comput. Assist. Tomogr. **21**, 539 (1997).
[5] A. C. Kak, and M. Slaney, *Principles of Computerized Tomographic Imaging* (IEEE Press, New York, 1987).
[6] H. Rauch and S. A. Werner, *Neutron Interferometry* (Oxford University Press, Oxford, 2000).
[7] M. Zawisky, Y. Hasegawa, H. Rauch, Z. Hradil, R. Myska, and J. Perina, J. Phys. A **31**, 551 (1998).
[8] L. A. Shepp and B. F. Logan, IEEE Trans. Nucl. Sci. **NS-21**, 21 (1974).
[9] J. Rehacek, Z. Hradil, M. Zawisky, W. Treimer, and M. Strobl, Europhys. Lett. **59**, 694 (2002).
[10] H. Rauch, J. Summhammer, M. Zawisky, and E. Jericha, Phys. Rev. A **42**, 3726 (1990).
[11] M. Zawisky, H. Rauch, and Y. Hasegawa, Phys. Rev. A **50**, 5000 (1994).
[12] J. F. Walkup and J. W. Goodman, J. Opt. Soc. Am. **63**, 399 (1973).
[13] S. L. Braunstein, J. Phys. A **25**, 3813 (1992).
[14] J. Řeháček, Z. Hradil, M. Zawisky, S. Pascazio, H. Rauch, and J. Peřina, Phys. Rev. A **60**, 473 (1999).
[15] V. F. Sears, Neutron News **3**, 26 (1992).
[16] M. Zawisky, U. Bonse, R. Loidl, Z. Hradil, and J. Řeháček, Europhys. Lett. **68**, 337 (2004).